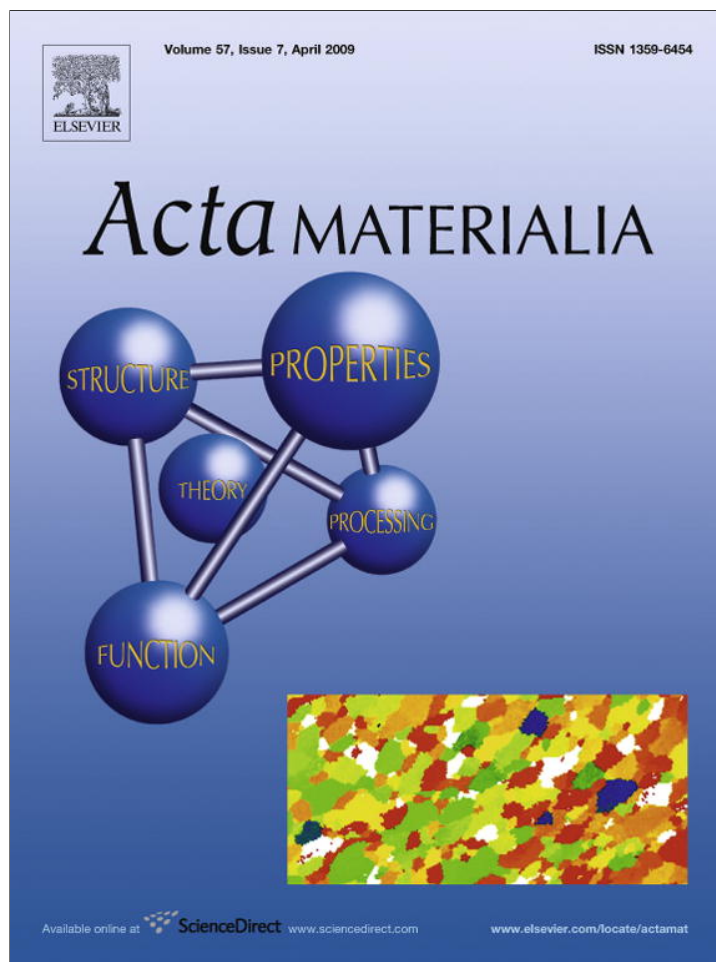


Provided for non-commercial research and education use.  
Not for reproduction, distribution or commercial use.



This article appeared in a journal published by Elsevier. The attached copy is furnished to the author for internal non-commercial research and education use, including for instruction at the authors institution and sharing with colleagues.

Other uses, including reproduction and distribution, or selling or licensing copies, or posting to personal, institutional or third party websites are prohibited.

In most cases authors are permitted to post their version of the article (e.g. in Word or Tex form) to their personal website or institutional repository. Authors requiring further information regarding Elsevier's archiving and manuscript policies are encouraged to visit:

<http://www.elsevier.com/copyright>



# Grain boundary shear–migration coupling—I. In situ TEM straining experiments in Al polycrystals

F. Momprou\*, D. Caillard, M. Legros

*CEMES-CNRS, BP 4347, 31055 Toulouse Cedex, France*

Received 18 December 2008; received in revised form 15 January 2009; accepted 15 January 2009

Available online 2 March 2009

## Abstract

Grain boundary (GB) migration was dynamically observed and characterized by means of in situ transmission electron microscopy straining experiments at moderate temperature in ultrafine grain aluminium. This motion is a response to the applied external stress, which leads to faceted fast growth of some grains at the expense of smaller ones. The combined use of fiducial markers and image correlation made possible a measure of strain associated with GB migration. The crystallographic orientation of both sides of moving GB was simultaneously recorded. The shear produced by the observed migration was thus estimated, leading to a coupling factor close to 20%. These results are discussed and compared with existing models describing the coupling between shear stress and GB migration. © 2009 Acta Materialia Inc. Published by Elsevier Ltd. All rights reserved.

**Keywords:** Transmission electron microscopy (TEM); Aluminium; Grain boundary migration; Plastic deformation; Ultrafine grained microstructure

## 1. Introduction

The influence of grain boundaries (GB) on the mechanical properties of crystalline materials is a wide and still open research area in materials science. When the grain size is severely reduced as in ultrafine-grained (UFG) or nanocrystalline (nc) metals, understanding the role of the GB becomes critical. Because both the mean free path and the probability of multiplication of dislocation are constrained, a probable change in the plasticity mechanism associated with very high yield stresses is bound to occur below a critical grain size [1]. This change in deformation process would result in the breakdown of the well-known Hall–Petch hardening law for grain size smaller than a few nanometres [1,2]. Because exploring these mechanisms in agglomerates of very small crystallites is physically extremely complex, a vast number of computer-simulated experiments have pointed to several alternative deformation processes (for reviews, see Refs. [3] and [4]). Most of them originate from GB because of the very high volumic frac-

tion of GB in these simulated polycrystals and the associated high stresses due to the lack of easy dislocation glide. If some of these alternative mechanisms still involve perfect or partial dislocations through limited nucleation or absorption at GB [5], plasticity could also be carried out by the sole motion of GB [6]. Indeed, collective GB-based mechanisms [7] can potentially account for much larger deformation in very small-grain-sized metals than dislocation-based processes can [8].

Plasticity mechanisms directly connected to GB motion can be of several kinds. To a large extent, earlier work focused on GB sliding and grain rotation in order to account for superplasticity [9,10]. In contrast, the stress-induced migration of GB, although known for a long time, has never been recognized as a plasticity mechanism *per se* until the recent experiments in nanograined materials [11] and atomistic modelling [12].

GB migration was originally considered in high-temperature recrystallization mechanisms. Then, and because recrystallization generally yields no plastic deformation, boundary migration was assumed to be insensitive to externally applied stress. Alternatively, boundary migration was considered to be driven exclusively by the decrease in the

\* Corresponding author.

E-mail address: [momprou@cemes.fr](mailto:momprou@cemes.fr) (F. Momprou).

total boundary surface and by the decrease in the density of dislocations absorbed during the process. The migration process was thus interpreted in terms of the simple transfer of atoms from one grain to the other, with no associated shear displacement [13]. This stress-independent migration process has been subsequently observed by Babcock and Balluffi [14], and described by the more sophisticated shuffling model. In this case, groups of atoms are assumed to rotate in each unit cell of the coincidence site lattice (CSL) independently, which of course yield no deformation. More recent experiments and simulations have provided some evidence in support of the shuffling model [15–17].

The two hypotheses mentioned above—sliding with no migration and migration with no sliding—are so contradictory that they rather appear as two particular cases of a more general stress-induced migration process. Stress-induced boundary motion has actually been observed in several bi-crystals: of NaCl by Guillopé and Poirier [18], of Al by Fukutomi et al. [19], of Zn by Sheikh-Ali and Spuner [20], of cubic zirconia by Yoshida et al. [21], and of Au by Babcock and Baluffi [14]. As these bi-crystals were in coincidence orientation relationships, the boundary motions could be interpreted in terms of the displacement shift complete (DSC) dislocation model. In this case, plastic deformation results from the motion of DSC dislocations associated with steps (also called disconnections) in the interface plane. This plastic deformation can be a shear associated with a glide motion of DSC dislocations [18,20–22] or a deformation associated with a climb motion of DSC dislocations [23]. In the case of a pure shear deformation resulting from the migration of a pure tilt boundary, the shear direction is parallel to the boundary plane, and perpendicular to the rotation axis. The corresponding shear–coupling factor  $\beta$  is defined as the ratio of the shear displacement to the migration distance. Its value ranges between a few per cent and several tens per cent, depending on the length of the DSC Burgers vector and on the associated step height.

More recent experiments in Al bi-crystals by Winning et al. [24] and Molodov et al. [25] confirm the above results. They are, however, interpreted in terms of the alternative model of Cahn [26], where symmetrical tilt high-angle boundaries are described in the same way as low-angle ones, i.e. by an array of perfect edge dislocations. Under such a condition, migration occurs by the motion of these dislocations, in the glide planes perpendicular to the boundary plane. This also results in a shear displacement parallel to the boundary plane and perpendicular to the rotation axis. In the case of coincidence orientation relationship, the coupling factors predicted by the Cahn model can also be deduced from the DSC dislocation model, but not reciprocally. Indeed, in this case the Cahn model yields high  $\beta$  values, typically of several tens per cent, whereas the DSC dislocation model yields a larger spectrum of values. The model of Cahn is also supported by molecular dynamic simulations [27,28].

It is important to note that both the above shear–migration coupling mechanisms correspond to very specific situations of either coincidence or symmetrical tilt boundaries (DSC and Cahn models, respectively). They are accordingly not applicable to random boundaries like those present in polycrystals. In spite of this restriction, several recent deformation experiments have shown that stress-assisted grain growth is an active process in micro- and nanocrystalline metals, from moderate down to liquid nitrogen temperatures. These experiments were carried out by indentation in Cu [29], microtesting experiments and transmission electron microscopy (TEM) in situ straining experiments, in nanocrystalline Al thin films [11,30], high-pressure torsion and uniaxial tensile deformation of bulky nc-Al [31,32], and thermal cycling fatigue in microcrystalline Al [33].

In all these situations, stress-induced boundary migration is much more complex than in bi-crystals, because GB have random planes and misorientation angles, coupling factors at adjacent boundaries must be compatible, and triple junctions and GB curvature can play an important role. It is thus necessary (i) to characterize the coupling factors in polycrystals and relate them to the local microstructure (GB plane, misorientation) and (ii) to extend the available models to more general GB.

The second point is treated in Part II of this study. Concerning the first point, much of the difficulty in investigating nanocrystallized materials is due to the lack of suitable means of observing the dynamical response of a mechanical solicitation with sufficient spatial and time resolution. Such a task could be much more easily done in polycrystals with larger grains, as shown in the following. As the nature of the GB does not change down to the nanometre scale [34], the present investigation is fully transferable to nanocrystalline metals.

This paper reports on the qualitative and quantitative results on stress-assisted grain growth by means of in situ TEM straining experiments at moderate temperatures in UFG aluminium with micron-size grains. The approach consists in using fiducial markers and direct observation of large GB migrations to investigate the role of GB motion in strain accommodation processes. In order to reduce the critical stress for GB migration, and to minimize the intragranular dislocation activity, the experiments were carried out at a moderate temperature ( $\sim 350$  °C).

## 2. Experimental

Commercial purity (99.5%) UFG aluminium rods were produced by equal channel angular pressing after eight passes. More insight about the UFG Al preparation can be found in Refs. [35] and [36]. The mean grain size was  $\sim 800$  nm with no texture. In situ experiments were carried out using a custom-made high-temperature straining holder in a JEOL 2010 microscope operated at 200 kV. Rectangular samples were cut in a massive ingot and prepared by electrochemical polishing for TEM observations.

GB motion was monitored by means of DVD/HD recording using a MEGAVIEW II CCD camera. In all the displayed micrographs, the sample holder axis, also corresponding to the straining direction, is vertical. Electron diffraction was extensively used during the experiments in order to determine the crystallographic orientations of migrating and receding grains.

### 3. Results

#### 3.1. General aspect of stress-assisted GB motion

At room temperature, micro-samples exhibit grains with an average size of 800 nm, almost free from dislocations and containing some sub-GB. These micro-samples are first heated directly up to 300 °C, and then more slowly by 10 °C steps, until the very beginning of grain growth. Then, the temperature is kept constant until grain growth stopped. At that point, it is supposed that GB and triple points have reached an equilibrium state. A plastic strain is then imposed on the sample for a few seconds, and the applied stress is eventually allowed to relax before repeating the process. After each increment of strain, GB motion started and could be followed, as shown in Fig. 1 (see Appendix).

This figure shows a large growing grain with several curved facets. The grain growth, directed toward the concavity of the facets, starts under the application of the external stress by a rapid motion of the right-hand side GB at a speed of  $2 \mu\text{m s}^{-1}$  (Fig. 1b and c). Then, the upper boundaries go on migrating at a lower speed close to  $10 \text{ nm s}^{-1}$  (Fig. 1d). The motion of GB eventually stops, probably because part of the applied stress has been relaxed. The correlation between GB motion and stress has been examined in several experiments: in all cases, GB start to move as soon as an increment of stress is applied and stop after the stress is relaxed. The motion appears to be viscous with a concomitant motion of both GB and triple junctions. The fast GB motion between Fig. 1a and b seems to be associated with the small radius of curvature of the lower GB on the right-hand side. In the same way, the increase in GB speed between Fig. 1b and c is correlated to a 10% decrease in the corresponding concave radii of curvature. This indicates that capillary forces have a substantial contribution in GB migration.

Fig. 1e shows a picture taken in another area where a growing grain, on the left-hand side of the image, has swept the adjacent grain to the right. The GB appears as a thick black line with a width ( $d$ ) corresponding to its projection in the observation plane. In the present case, the apparent width is much smaller (50 nm) than the sample thickness (300 nm), indicating that the GB plane is almost edge on. The picture also exhibits 3 lines (labelled tr.), each of them with two parallel black and white contrasts, more clearly visible in the inserts where contrasts have been enhanced. These contrasts arise from thermal grooving [37], a diffusion process that enables equilibrium of the surface ten-

sions at the top and bottom surfaces of the foil when GB are immobile. After the migration of the GB, the grooves tend to vanish but are never completely erased, presumably owing to surface oxidation. Under such conditions, the black and white contrasts correspond to the two opposite grooves on both surfaces, and the fact that several grooves are observed indicates that the GB has moved jerkily, being immobile long enough to enable sufficient grooving between each displacement. This jerky motion arises from variations in the local stress as a result of successive relaxations. The fact that the distance between black and white traces on opposite surfaces is not constant indicates that the GB habit plane has changed during the migration, and eventually led to an almost edge-on plane.

Fig. 2 shows an assembly of 10 grains labelled G1–G10 (Fig. 2a). One can also note several precipitates (see, for instance, those labelled X1–X3) which will act as fiducial markers. After the application of the stress (reminder: the straining axis labelled T is vertical on the figures), grain G1 starts growing by the migration of its left-hand boundary towards grains G5, G6 and G7. In the meantime, the bottom GB of grains G8 and G9 also migrate toward G7, which results in the complete shrinkage of grain G7 (Fig. 2b). The GB motion then stops as a result of the relaxation of the applied stress. After applying a second increment of plastic strain, the GB between G1 and G5 moves toward G5, which leads to the complete shrinkage of G5 (Fig. 2c). In Fig. 2d, G1 continues to grow at the expense of G3 and G4 and eventually stops. Then, G9 and G10 start to grow, leading to the shrinkage of G1 and G2 (Fig. 2e and f). At that point, many dislocations nucleate and move in the interior of G9 and G10, and no further GB motion can be seen. The growth of G1 and its subsequent shrinkage are seen in Fig. 2g and h, where the successive GB positions are superimposed. This experiment is characteristic of many other similar stress-induced GB migrations that have been recorded.

All GB motions take place at a velocity of a few hundred nanometres per second, before stopping. Rapid migration seems to be directly correlated to the shrinkage of small grains. Indeed, as the grain shrinks, its GB are more and more curved and, as a result, their migration is faster. This result indicates that GB migration is driven both by the applied stress and by capillarity forces due to GB curvature.

From these experiments, orientations of growing grains along directions perpendicular to the foil planes and parallel to the straining axis, respectively, have been reported on the inverse pole figures of Fig. 3a and b. A random distribution throughout the triangle is observed in both cases, indicating that no texture is favoured during grain growth. This is in agreement with results obtained on deformed aluminium freestanding nanocrystalline thin films [43].

From another experiment, Fig. 4a and b shows faint contrasts, moving rapidly ( $\sim 150 \text{ nm s}^{-1}$ ) in the interface between two grains labelled G1 and G2 (see Appendix). These contrasts seem to be related to dislocations moving

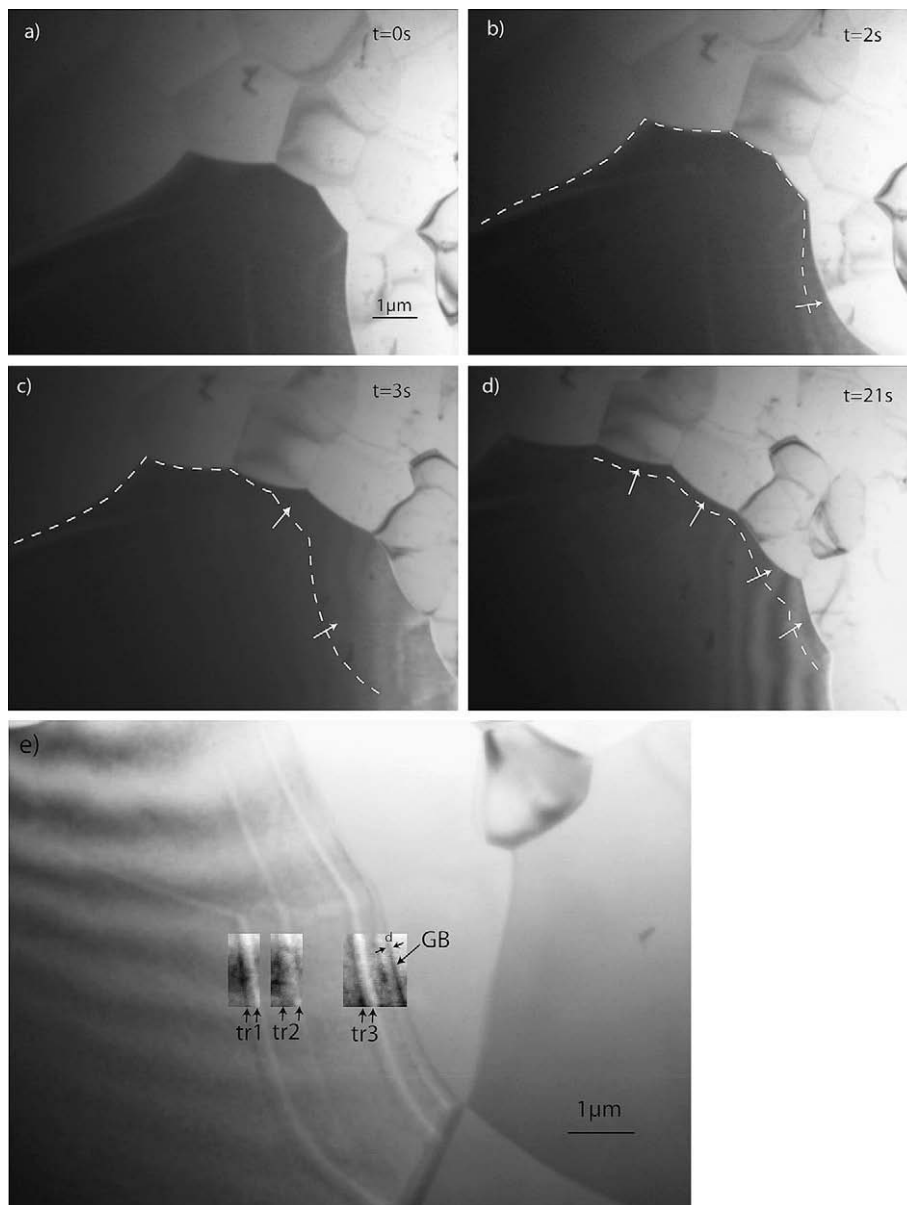


Fig. 1. (a–d) Grain growth under external applied stress recorded during in situ straining experiments at 350 °C. The straining axis ( $T$ ) is vertical in the pictures. The growing grain seen here in dark exhibits several curved facets. White dashed lines indicate GB positions as they are on the preceding image. Note between (b) and (c) a rapid GB motion at  $1 \mu\text{m s}^{-1}$ . (e) Image showing surface traces (denoted tr.) left at different times by a GB after its migration. Contrast was enhanced in some area in order to see traces on both top and bottom surfaces (black and white parallel traces).

in the GB plane as a result of the migration of the GB shown in Fig. 4c. Also note that this strong dislocation activity is confined to the GB habit plane, which is not a priori a (111) plane.

Fig. 5 shows another typical stress-assisted grain growth where four grains (labelled G1–G4) are involved. Each of them has fiducial markers labelled X1–X4 (see Appendix). Under stress, G2 grows at the expense of G3 (Fig. 5b and c). Then, G1 grows suddenly, which leads to the shrinkage of G4 (Fig. 5c and d). As previously, this motion is accelerated by a rapid increase in the GB surface tension force as the receding grain shrinks. The next section shows, from this sequence, how to measure strain associated with GB migration.

### 3.2. Strain measurement

Fig. 6 shows strain measurements performed on an enlarged area of Fig. 5. In each figure, two pictures taken before and after GB migration have been superimposed, and their contrasts have been subtracted. This allows a precise superposition of both images of a given grain, by minimizing the contrast of the corresponding markers. The best image superposition in G2 is obtained when the contrast of marker X2 is minimum. Such image correlation allows the GB to be located before and after migration and measurement of the corresponding plastic deformation. The GB between G1 and G2 (labelled GB12) has first moved from position A to position B (Fig. 6a) and from B

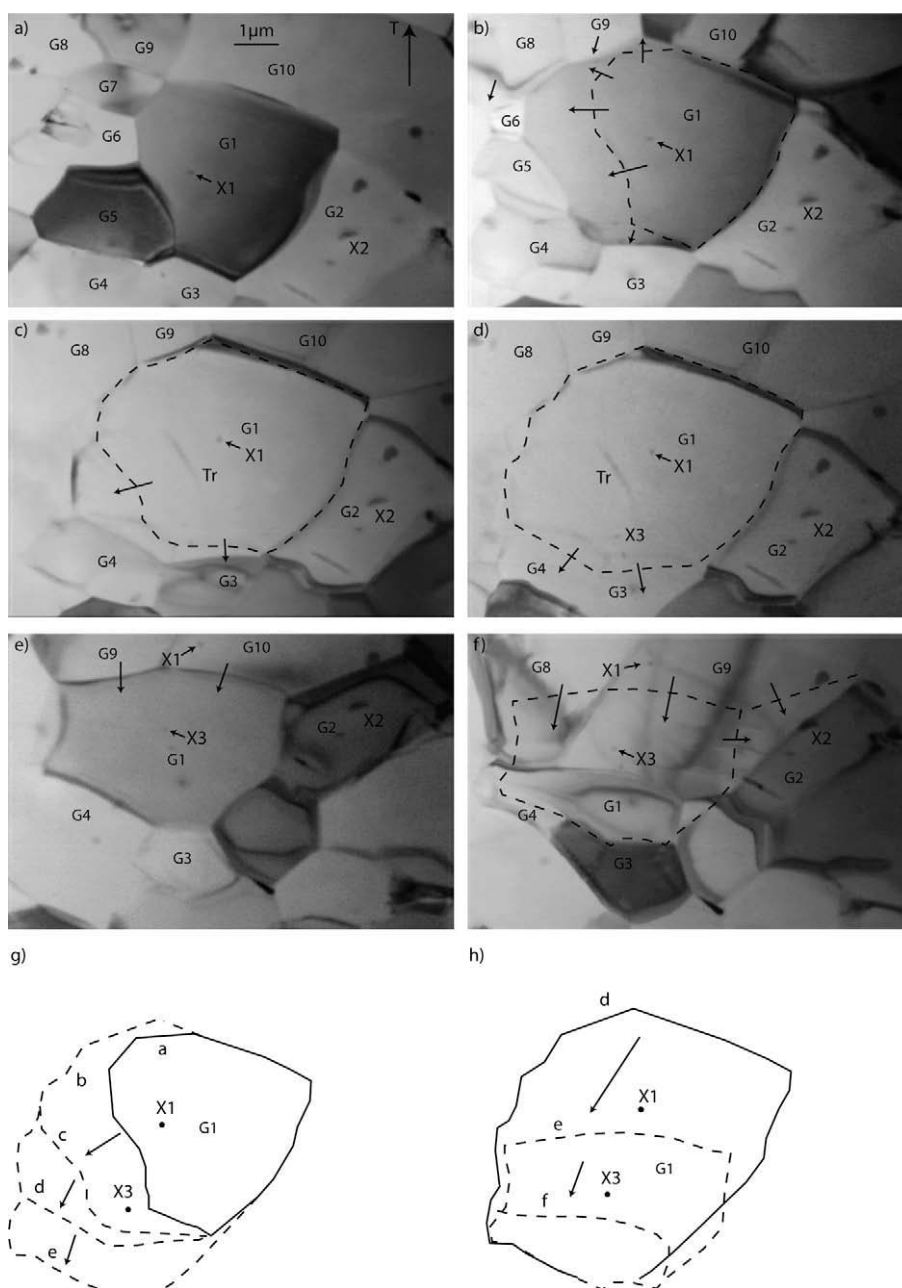


Fig. 2. Stress-assisted grain growth followed in an assembly of 10 grains labelled G1–G10. In the first step, G1 grows (a–e), leading to the shrinkage of adjacent grains G5 and G6. In the second step (e–f), G1 recedes owing to the growth of G8 and G9. These two steps are schematized in (g) and (h). Note the presence of precipitates labelled X1, X2 and X3, which act as fiducial markers.

to C (Fig. 6b) in a second step. The change in trace direction and apparent width of GB12 indicates that its habit plane has changed during migration. This is similar to what is observed in Fig. 2d.

As G2 is rigid, as a result of the absence of any intergranular dislocation motion, attention is focused on the displacement of fiducial markers outside G2. Fig. 6c, which is an image correlation between positions A and C, shows that markers have been shifted after the GB has passed (note their initial positions in white and their final ones in black in areas where the contrast has been reinforced). This indicates that the lattice surrounding the markers

has been subjected to deformation. Moreover, a change in the direction of deformation can be observed between Fig. 6a and b because the projected direction of the deformation, indicated by arrows joining the markers' positions, is first inclined with respect to the GB trace (dashed line A in Fig. 6a) and then parallel to the GB traces (dashed lines B and C in Fig. 6b). Lastly, the inspection of all markers shows that the apparent displacement ( $s_a$ ) increases as a function of the distance ( $m_a$ ) to the interface, between positions A and C, and remains constant behind position A. This can be explained by considering a migration-induced plastic deformation, as shown in Fig. 6d. The apparent

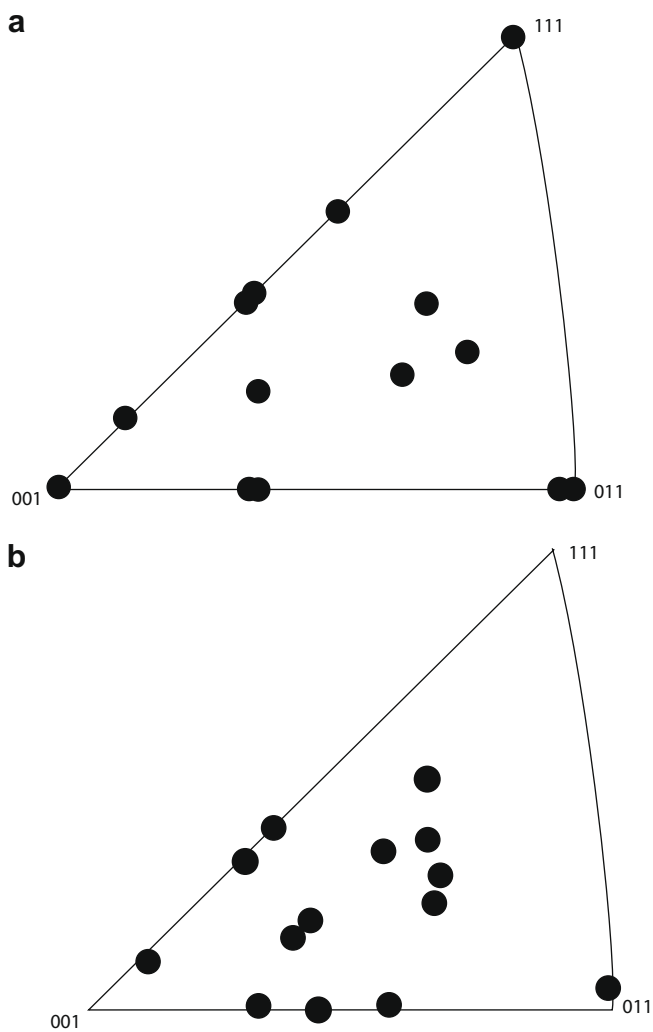


Fig. 3. Inverse pole figure showing directions (a) parallel to foil surface and (b) parallel to the straining axis, for growing grains.

coupling factor ( $\beta_a$ ) is the ratio between the apparent displacement ( $s_a$ ) and the apparent distance perpendicular to the interface ( $m_a$ ). Values of  $s_a$  as a function of  $m_a$  between A and C, are reported in Fig. 6e and fitted by a linear plot. The slope of this linear plot corresponds to the mean value of  $\beta_{a(A-C)}$  for the whole GB migration. In this figure,

$\beta_{a(A-C)}$  is  $\sim 6\%$ . Intermediate values between positions A and B, on the one hand, and B and C, on the other hand, lead to  $\beta_{a(A-B)} \approx 7\text{--}10\%$  and  $\beta_{a(B-C)} \approx 9\%$ , respectively. These two latter values are larger than  $\beta_{a(A-C)}$  because they partly cancel. The deformation measured in a previous study is of the same order of magnitude [38].

The successive habit planes of GB12 have been deduced from their trace directions, and from the variation in their apparent widths with tilt angle. They are located in the shaded area of the stereographic projection in Fig. 7. The large circle of the stereographic projection corresponds to the foil surface of the sample. The plane noted P(A–B) refers to GB12 between positions A and B, and P(B–C) to GB12 between positions B and C. The corresponding plane normals, denoted  $\mathbf{n}(A-B)$  and  $\mathbf{n}(A-C)$ , are also reported. Fig. 7 also shows the relative grain orientations G2 (opened symbol)/G1 (filled symbol).

As GB12 is almost edge on between positions B and C (note the very small apparent width of GB12 in position C in Fig. 6b), and as the corresponding marker displacements are parallel to the traces, the deformation is necessarily a pure shear parallel to the GB plane. As GB12 is more inclined between positions A and B (Fig. 6a), one cannot use similar arguments and cannot determine which kind of deformation occurred in this case. In particular, the deformation could involve some component of long-range diffusion. However, as the kinetics of GB migration is almost the same between A and B and between B and C, one can reasonably think that the motion is controlled by a single process, which is thus necessarily a pure shear deformation. This point will be discussed again in Section 4.3. With this hypothesis, it is then possible to identify the shear direction between positions A and B,  $\mathbf{s}_{a(A-B)}$ , with the direction of the GB plane which projects in the observation plane along  $\mathbf{s}_{a(A-B)}$  (Fig. 7). The shear direction between B and C,  $\mathbf{s}_{a(B-C)}$ , cannot be determined similarly because  $\mathbf{s}_{a(B-C)}$  is too close to the trace of GB12.

#### 4. Discussion

In the present work, the migration of several GB with random planes and misorientations was observed in

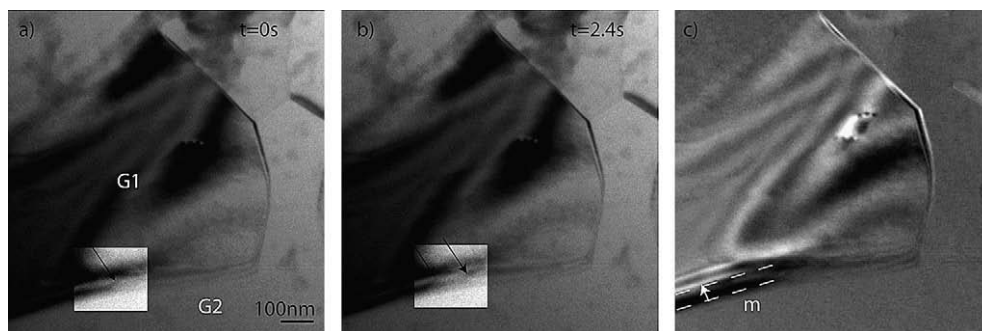


Fig. 4. (a and b) Pictures showing dislocation motions in a moving GB plane. Areas where GB dislocations are visible have been lightened. (c) Image superimposition showing the amplitude ( $m$ ) of GB migration.

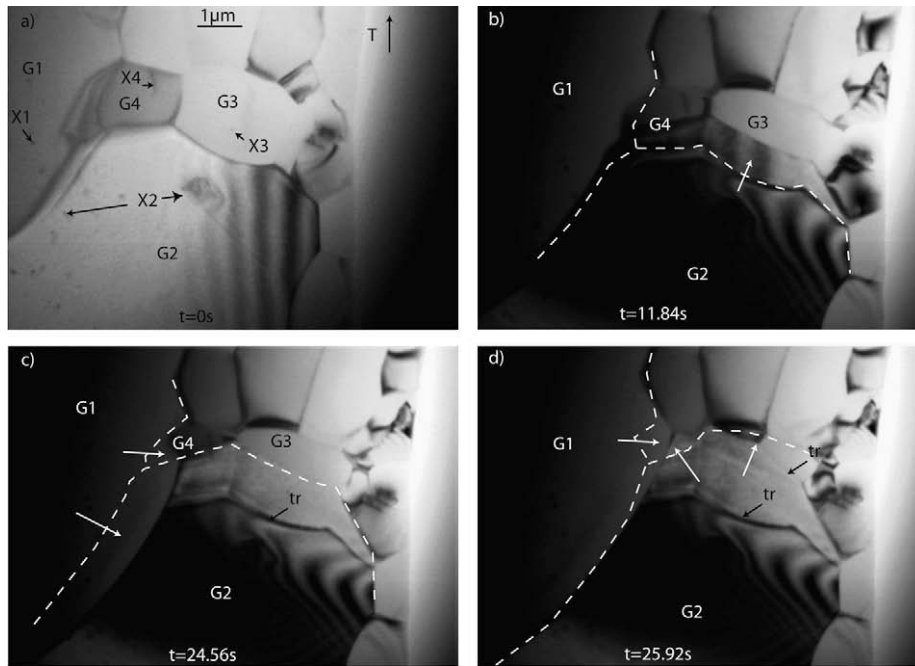


Fig. 5. Images showing GB migration under stress. G2 grows first at the expense of G3 (a–d). Note the groove in Fig. 5c (tr.) left by GB23 (the GB between G2 and G3) in Fig. 5a. In (c) and (d), the GB between G1 and G2 starts to move, leading to the shrinkage of G4. During this process, markers X3 and X4 are swept by the GB.

micron-grained aluminium strained in situ at moderate temperature ( $\sim 350^\circ\text{C}$ ). GB migration is clearly a stress-assisted process, because it consistently starts with the application of stress, ceases as soon as the stress is relaxed, and starts again as soon as a new increment of stress is applied.

The different aspects of GB mobility are now discussed.

#### 4.1. GB migration under surface tension effects

The surface tension due to the curvature of GB obviously contributes to their motion. The concave curvature observed on GB in Fig. 1a–d can be explained considering that grains with a number of facets larger than six (note that the growing grain of Fig. 1d has seven visible facets) must have concave GB in order to achieve equilibrium between surface tension forces at triple points (Fig. 8). The concavity in turn imposes the grain to grow [39,40], because the force  $\mathbf{F}_i$  directed on each point of the GB toward the centre of the curvature drives a GB motion toward the concavity. As soon as this motion occurs, the curvature decreases and, in order to maintain  $120^\circ$  angles, triple points have to migrate in turn. Thus, a dynamic equilibrium between the motion of GB and triple points is attained. As the force  $\mathbf{F}_i$  is inversely proportional to the radius of curvature, facets with the smallest radius of curvature will be the fastest, as observed in the present experiments (see, for example, GB on the right-hand side of Fig. 1c). As the facets expand, the radius of curvature increases (Fig. 8 at time  $t_1$ ), and then the growth is slowed down. This mechanism can account for grain growth even in the absence of any external stress (pure recrystallization).

#### 4.2. GB migration under an externally applied stress

When an external force is applied, the dynamic equilibrium is still maintained but the velocity of GB and triple points increases. Under stress, one can assume that the mobility depends on the nature of GB. For a pure tilt GB, the misorientation is around an axis  $\mathbf{R}$  contained in the GB plane, and the shear  $\mathbf{s}$  associated with the GB migration is perpendicular to  $\mathbf{R}$  and parallel to the GB plane (Fig. 9a). Let  $\gamma = (\sigma, \mathbf{n})$  be the angle between the applied stress direction and the normal to the GB plane, and  $\varphi = (\sigma, \mathbf{s})$  the angle between the applied stress direction and the shear direction. In a bi-crystal of section  $S_0$ , and for an amount of shear  $s$ , the work done by the migrating boundary is  $\sigma S_0 s \cos \gamma$ . This is equal to the work done by the driving stress  $\sigma_d$  per unit surface on the boundary, over the area  $S_0 / \cos \varphi$ , and over the distance  $m$ . The driving stress is then

$$\sigma_d = \sigma \beta \cos \gamma \cdot \cos \varphi \quad (1)$$

where  $\beta$  is the coupling factor ( $\beta = s/m$ ). The corresponding Schmid factor is

$$m_s = \sigma_d / \sigma = \beta \cos \gamma \cdot \cos \varphi \quad (2)$$

As  $(\mathbf{n}, \mathbf{s}) = 90^\circ$ , the maximum Schmid factor is equal to  $0.5\beta$ .

A mixed GB can be deduced from a pure tilt one by rotating the GB plane around  $\mathbf{s}$  by an angle  $\delta$  in such a way that the misorientation axis  $\mathbf{R}$  no longer belongs to the GB plane (Fig. 9b).

The shear produced by the normal motion of this mixed GB over a distance  $m'$  is equal to the shear  $s$  produced by

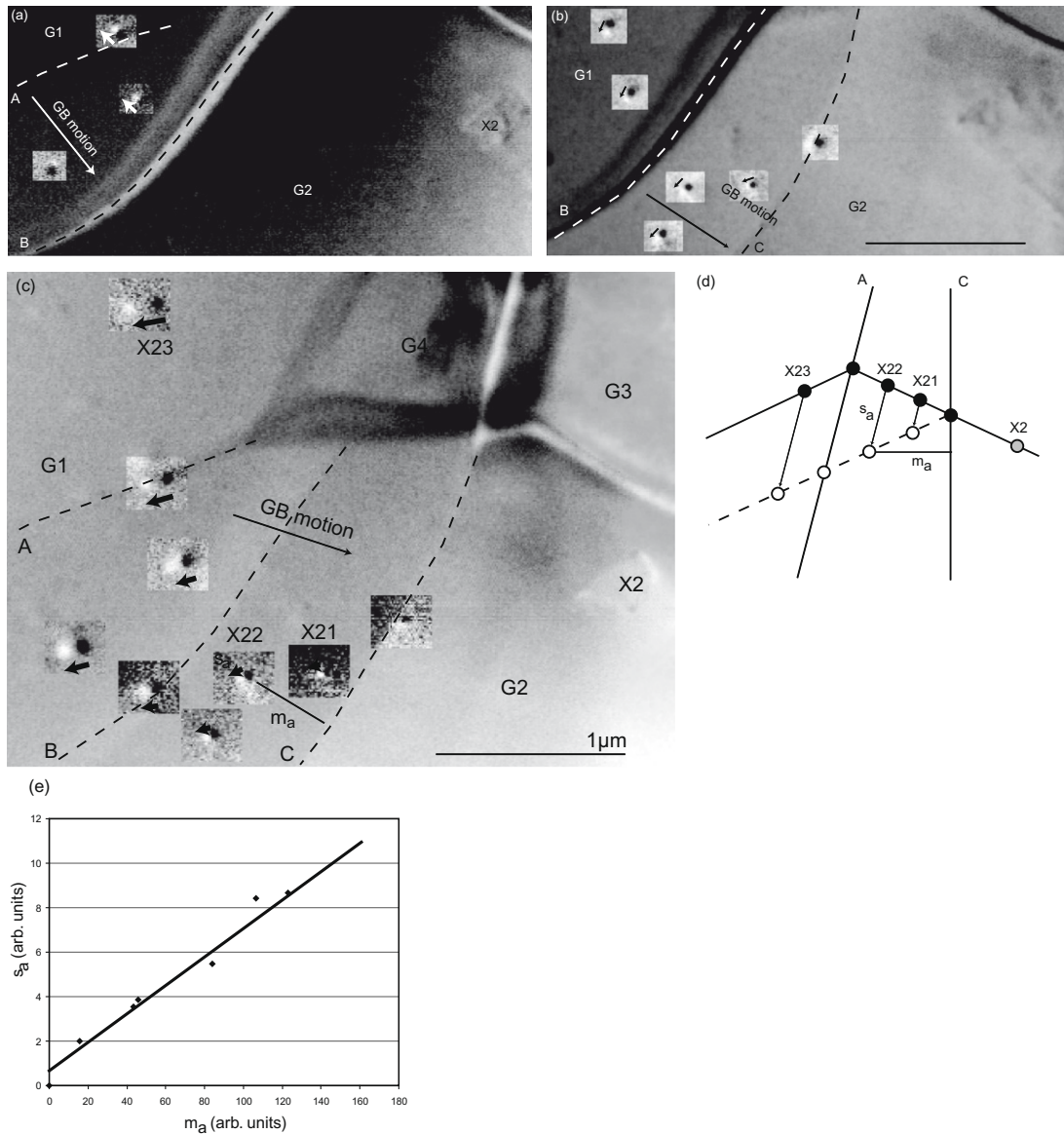


Fig. 6. (a–c) Image correlation associated with the GB motion between G1 and G2 obtained for different GB positions: between position (a) A and B, (b) B and C, (c) A and C. The images are obtained by superimposing X2 markers on two pictures with opposite contrasts taken before and after GB motion. Marker displacements in adjacent grains (note that black and white contrasts do not overlap) indicate a deformation. (d) Schematized description of the migration and the coupling between apparent shear  $s_a$  and apparent migration  $m_a$ , explaining markers' displacement. (e) Experimental measurement extracted from (c) of  $s_a$  vs  $m_a$ . The linear fit gives a value of the apparent coupling factor  $\beta_a$ .

the motion of the pure tilt component of the GB on the distance  $m' \cos \delta$ . Then, the corresponding coupling factor is

$$\beta' = \frac{s'}{m'} = \frac{\beta m' \cos \delta}{m'} = \beta \cos \delta \quad (3)$$

where  $\beta$  is the coupling factor of the corresponding pure tilt GB.

The corresponding Schmid factor:

$$m'_s = \beta \cos \delta \cdot \cos \gamma \cdot \cos \varphi \quad (4)$$

is lower than for a pure tilt boundary. Under such conditions, GB with the largest tilt component should have the largest driving force.

#### 4.3. Evaluation of $\beta$ and interpretation

For a given misorientation between two grains, a large choice of rotations  $\mathbf{R}$  connecting them is offered. In Fig. 7, those corresponding to the misorientation between grains 1 and 2 are represented by crosses. To each vector  $\mathbf{R}$  corresponds a possible shear direction  $\mathbf{s}$ , perpendicular to  $\mathbf{R}$ , and parallel to the GB plane. Only the rotation axes close to the GB plane, i.e. for which there is a large tilt component, are consistent with stress-induced migration. Nevertheless, the multiplicity of the possible directions of  $\mathbf{R}$  and  $\mathbf{s}$  can account for the change in shear direction in association with a change in GB plane, observed in Fig. 6.

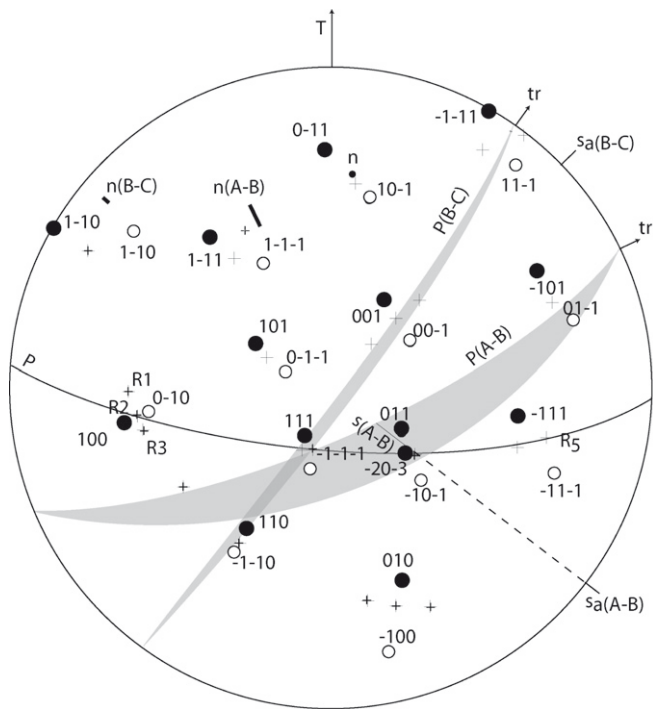


Fig. 7. Stereographic projection showing orientation of G1 (opened symbol) and G2 (filled symbol). One orientation can be deduced from the other by an adequate rotation along axes indicated by crosses. GB planes associated with A–B and B–C GB motion (see Fig. 6) are shown as shaded areas. Shear direction  $s_{(A-B)}$  corresponds to the intersection of the projected shear direction and the GB planes. Almost tilt GB compatible with the shear direction measured experimentally ( $s_{a(A-B)}$ ) correspond to the three possible rotation axes  $R_1$ ,  $R_2$  and  $R_3$  and the corresponding shear direction  $s_{(a-b)}$ . The plane P is the corresponding pure tilt GB containing the shear direction  $[-20-3]$  and  $R_2$ .

Strain measurement enables one to discuss the different models proposed in the literature.

The role of diffusion in GB migration must first be discussed. Long-range diffusion cannot be ruled out at temperatures where the experiments were performed. However, the sole diffusion cannot explain the high GB speed observed (a few hundred nanometres per second). For instance, one can estimate GB speed due to diffusion from the Coble creep equation:

$$v = \dot{\epsilon}d = 14\pi \frac{\sigma\Omega}{kT} \frac{\delta D_b}{d^2} \quad (5)$$

Taking  $\sigma \approx 100$  MPa the applied stress,  $\Omega \approx 0.7b^3$  (with  $b \approx 0.29$  nm),  $T = 350$  °C, mean grain size  $d = 800$  nm and  $\delta D_b = 4.3410^{-25}$  m<sup>3</sup> s<sup>-1</sup> [41] (with  $\delta$  the GB width, and  $D_b$  the GB diffusivity), this leads to  $v \approx 10^{-12}$  m s<sup>-1</sup>. This value is far smaller than the observed speed (up to  $2 \times 10^{-2}$  m s<sup>-1</sup>, for instance, in Fig. 1). The fact that fast GB migration under stress could not be explained by long-range diffusion processes has also been confirmed in several numerical simulations [6,42] and recent experiments in nc-Al [43]. The migration mechanism observed is thus clearly conservative, in agreement with the shear displacements measured in Section 3.2. Some long-range diffusion

could be invoked, however, in order to relax local strain incompatibilities, especially at triple junctions. Short-range diffusion as in shuffling mechanism is also likely to occur.

Among the different conservative processes discussed in Section 1, the pure shuffling one [23] can be ruled out, because the migration observed in the present study is stress assisted and results in some quantified plastic deformation.

Such a shear deformation is predictable within the framework of DSC dislocation and Cahn's models [26] and, in order to compare the present results with these models, it is now necessary to evaluate the value of the real coupling factor  $\beta$ , in the case of Figs. 6 and 7. Fig. 10 shows the relation between the real values of  $s$ ,  $m$ ,  $\beta$  and their apparent counterparts. The estimation of the real migration distance takes into account the inclination  $\alpha$  of the GB plane with respect to the foil plane normal. However, the real shear displacement depends on the angle  $\phi$  with its projected measured value. Thus, the coupling factor is given by

$$\beta = \frac{\beta_a}{\cos \phi \cos \alpha} \quad (6)$$

The choice of a rotation axis perpendicular to direction  $s_{(A-B)}$  determined in Section 3.2, and for which the GB has a large tilt component, leads to three rotation axes labelled  $R_1 = [1-13-1]$ ,  $R_2 = [0-15-1]$  and  $R_3 = [-1-17-1]$  leading, respectively, to a misorientation of 75°, 164.8° and 105.4° (Fig. 7). One can first remark that these rotation axes do not correspond to a low index coincident GB. However, in order to compare results with existing theories which only rely on low index coincident GB, it will be assumed that directions  $[100]$  and  $[0-10]$  in the two crystals are parallel, and then that the rotation axis is  $R = [0-10]$  with a misorientation angle equal to 157.38° ( $\Sigma 13a$ ). This is reasonable, as the three possible rotations  $R_1$ ,  $R_2$  and  $R_3$  deviate only slightly from  $\Sigma 13a$  (theoretical rotation angles 67.38°, 157.38°, 112.62°). The case of non-coincident GB is discussed at the end of the paper. The shear direction  $s_{(A-B)}$ , which is the intersection of the plane normal to  $R$ , the GB plane and the projected shear direction, is found close to  $[-20-3]$ . Knowing that  $\beta_{a(A-B)} \approx 7-10\%$ , one can then deduce  $\beta$  from (1), with  $\phi = (s, s_a) 56^\circ$  and  $\alpha = 30^\circ$  measured in Fig. 7. One finally ends up with:  $\beta_{A-B} \approx 14-20\%$ .

For the sake of simplicity, the pure tilt GB containing  $s$  and  $R$  will be considered first. It will then be seen how the coupling factor has to be corrected for GB12. The pure tilt GB plane is shown in Fig. 7 and labelled P. As the normal  $n$  to P is a coincident direction (i.e.  $n$  is close to a possible rotation axis), the GB is almost symmetrical. Then, the migration can be described within the framework of both DSC dislocations model and Cahn's model.

Fig. 11 shows the  $\Sigma 13a$   $[0-10]$  pure tilt GB between two lattices represented by black and white spots. The CSL unit cell is also shown. Two DSC dislocations with Burgers vectors  $b_1$  and  $b_2$  are shown. They are parallel to the  $[-20-3]$  direction, in agreement with the observed shear direction.

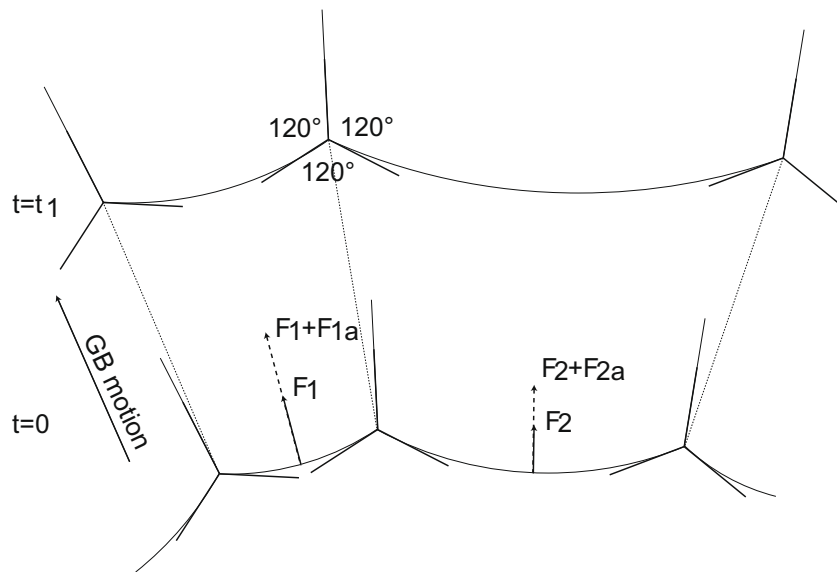


Fig. 8. Schematized evolution of GB facets under capillary forces ( $F_i$ ) and applied external forces ( $F_{ia}$ ) at two different times. Curved facets are expected to form in order to get  $120^\circ$  angles at triple points. The forces applied on the GB impose concomitant GB facets and triple points motion toward the concavity. Note that the GB facets expansion implies a decrease in the curvature and thus a decrease in grain growth velocity.

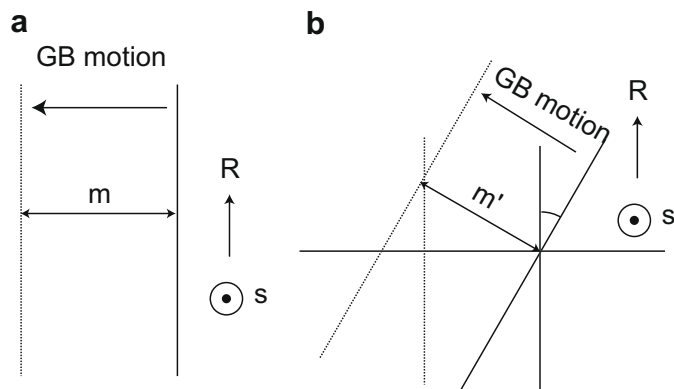


Fig. 9. Scheme showing that the coupling factor in (a) a pure tilt GB (s and  $\mathbf{R}$  parallel to the GB plane) is larger than that in (b) a mixed GB inclined by an angle  $\delta$  around s. The coupling factor in this latter case is equal to that corresponding to the motion of a pure tilt GB moving over the distance  $m' \cos \delta$ .

As the glide of these dislocations changes the origin of the CSL from A to C and from A to B, respectively, they introduce a step with height  $h$ . The corresponding coupling factor  $\beta$  is given by  $\beta = b/h$ .

This leads to  $\beta_1 = 40\%$  and  $\beta_2 = 25\%$ . The case of gliding dislocation with Burgers vector  $\mathbf{b}_1$  is of special interest, because it is equivalent to the  $[110]$  coupling mode proposed by Cahn [26]. Indeed, in this model, the  $[011]$  direction in the right-side grain is rotated clockwise by an angle  $\varphi = \frac{\pi}{2} - \theta$  ( $\theta$  being the misorientation angle) and becomes parallel to the  $[011]$  direction in the left-hand grain.

As GB12 is not a pure tilt boundary, the measured coupling factor has to be corrected in order to compare it with the theoretical values valid for pure tilt boundaries. Considering that the GB is inclined by an angle  $\delta = (n(\mathbf{A}-\mathbf{B}), n) = 28^\circ$  around the shear direction, the expected coupling factor in

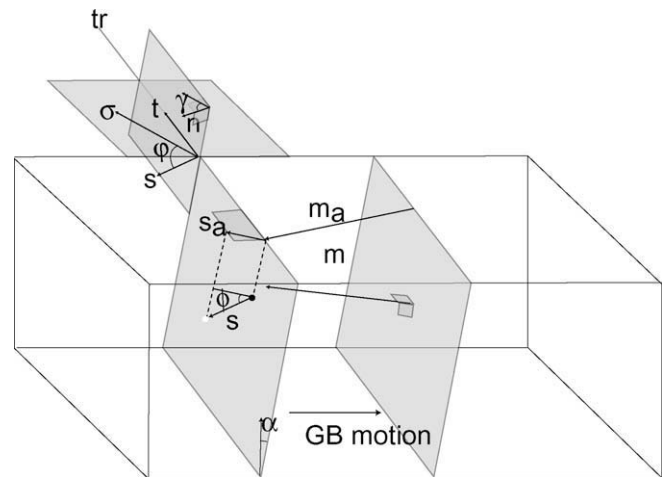


Fig. 10. Schematized description of GB motion showing the relation between real and apparent shear and migration.

the case where GB12 would be pure tilt is  $\beta = 14\text{--}20\% / \cos \delta \approx 16\text{--}23\%$  (see Section 4.2). This value is significantly smaller than that expected from Cahn's model ( $\beta_1 = 40\%$ ). The measured coupling factor is, however, close to  $\beta_2 = 25\%$  predicted by the DSC dislocation model.

Models involving the motion of GB dislocations in the GB plane (e.g. the DSC dislocation model) are also supported by the observation of dislocations moving rapidly at the GB interface shown in Fig. 4. Indeed, in  $\sim 13$  s, the GB has covered a migrating distance ( $m$ ) of 38 nm (Fig. 4c), and the corresponding number ( $n$ ) of passing dislocations is estimated to be of the order of 25. Taking  $b_{GB} \approx 0.15$  nm as a typical DSC dislocation Burgers vector (see, for instance, Rae and Smith [13]), a value of  $\beta_a = \frac{nb_{GB}}{m_a} = 7\%$  is obtained. Although it is difficult to count the dislocations accurately, especially when

GB move rapidly, this value is close to what was measured using markers in Fig. 6.

Until now, the approximation of a low index GB has been treated. This is reasonable, as the rotation axes  $R_1$ ,  $R_2$  and  $R_3$  only slightly deviate from a  $\Sigma 13a$  GB. However, this approximation is questionable. Could any other alternative mechanisms be invoked in the general case? It seems doubtful that shear-coupled GB migration can be strictly described within the framework of DSC dislocation model or Cahn's model, which both rely on the existence of an underlying CSL unit cell. In this general case, the rotation axis is arbitrary, the interface plane is irrational and the CSL unit becomes infinitely large. Then a model must be proposed for more general GB. This will be treated in Part II of this paper.

### 5. Conclusions

The following conclusions can be drawn from this study:

1. Strong evidences of stress-assisted grain growth was found in UFG aluminium by means of in situ TEM straining experiments.
2. The deformation associated with GB migration was measured using the superposition of surface markers. It clearly shows a coupling between shear and migration. In the case of a high-angle GB close to a low index GB, an apparent shear of 6–7%, resulting in a coupling factor of order 20% was measured.
3. In the case of a low index GB, the measured coupling factor can be explained within the framework of the DSC dislocation model. From the several cases observed and analysed so far, the coupling factor was generally found to be smaller than that predicted by the Cahn model [26]. The fact that existing coupling models such as Cahn's model yield a low number of coupling values only for coincidental GB suggests the need for a more elaborate analysis of the possible coupling modes for general tilt boundaries. This is developed in the second paper in this study.
4. GB motion was sometimes correlated with the motion of GB dislocations, in disagreement with the model of Cahn.
5. The present experiments were carried out at an intermediate temperature, and GB migrations occurred without emission of dislocations. This underlines the fact that

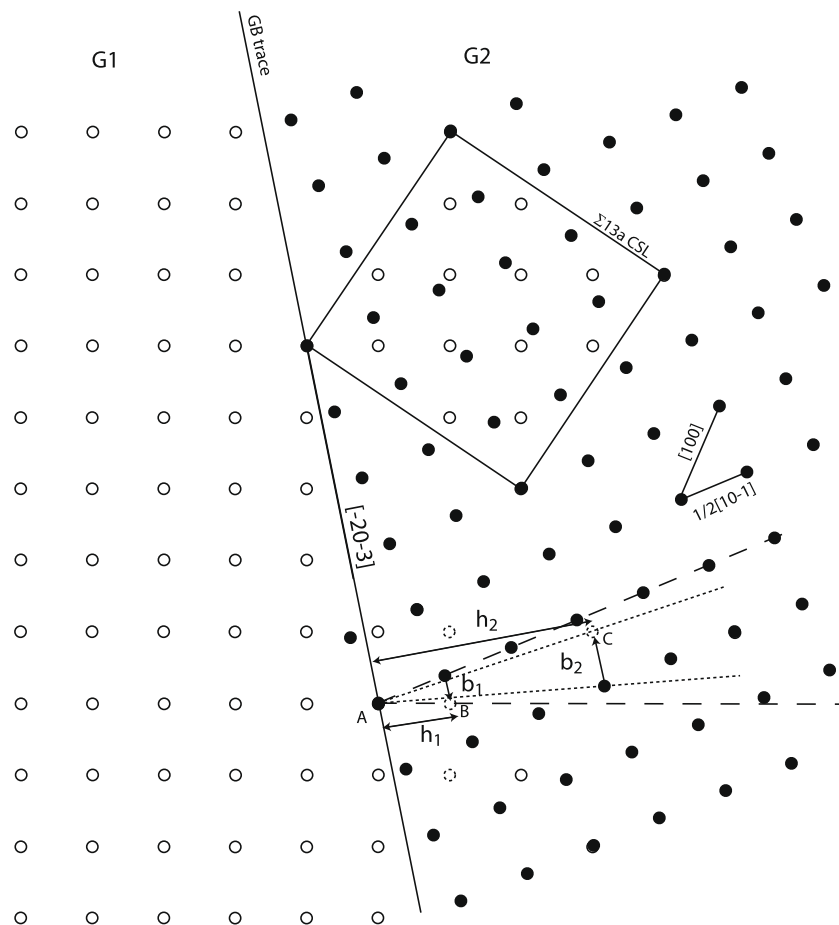


Fig. 11. Possible DSC dislocation mechanisms in a  $\Sigma 13a$   $[100]$  GB. Gliding dislocations with Burgers vectors  $b_1$  and  $b_2$  parallel to the interface leads to the normal GB motion over distances  $h_1$  and  $h_2$ , respectively.

diffusion should play a minor role in the resulting shear, but is needed at a very local scale to accommodate strain incompatibilities.

### Acknowledgments

The authors acknowledge Prof. H. Mughrabi for providing the UFG samples.

### Appendix A. Supplementary data

Video sequences relating to Figs. 1, 4 and 5 can be seen in the supplementary data associated with this paper, in the online version, at [doi:10.1016/j.actamat.2009.01.014](https://doi.org/10.1016/j.actamat.2009.01.014).

### References

- [1] Schiotz J, Jacobsen K. *Science* 2003;301:1359.
- [2] Trelewicz J, Schuh C. *Acta Mater* 2007;55:5958.
- [3] Van Swygenhoven H, Weertman J. *Mater Today* 2006;9:31.
- [4] Wolf D, Yamakov V, Phillpot S, Mukherjee A, Gleiter H. *Acta Mater* 2005;53:40.
- [5] Van Swygenhoven H, Derlet P, Froseth A. *Acta Mater* 2006;54:1983.
- [6] Farkas D, Froseth A, Van Swygenhoven H. *Scripta Mater* 2006;55:698.
- [7] Gutkin M, Mikaelyan K, Ovid'ko I. *Phys Solid State* 2008;50:1279.
- [8] Saada G, Verdier M, Dirras G. *Philos Mag* 2007;87:4892.
- [9] Mara N, Sergueeva A, Mara T, McFadden S, Mukherjee A. *Mater Sci Eng A* 2007;463:238–44.
- [10] Mukherjee AK. *Mater Sci Eng A* 2002;322:1–22.
- [11] Gianola D, Van Petegem S, Legros M, Brandstetter S, Van Swygenhoven H, Hemker K. *Acta Mater* 2006;54:2253–63.
- [12] Haslam A, Moldovan D, Yamakov V, Wolf D, Phillpot S, Gleiter H. *Acta Mater* 2003;51:2112.
- [13] Rae CM, Smith DA. *Philos Mag* 1980;A41:477.
- [14] Babcock SE, Balluffi RW. *Acta Metall* 1989;37:2357.
- [15] Zhang H, Srolovitz D. *Acta Mater* 2006;54:633.
- [16] Schönfelder B, Gottstein G, Shvindlerman L. *Acta Mater* 2005;53:1609.
- [17] Merkle KL, Thompson LJ, Phillipp F. *Phys Rev Lett* 2002;88:225501.
- [18] Guillope M, Poirier JP. *Acta Metall* 1980;28:163–7.
- [19] Fukutomi H, Iseki T, Endo T, Kamijo T. *Acta Metall Mater* 1991;39:1145.
- [20] Sheikh-Ali AD, Szpunar JA. *Mater Sci Eng A* 1998;245:49.
- [21] Yoshida H, Yokoyama K, Shibata N, Ikudara Y, Sakuma T. *Acta Mater* 2004;52:2349.
- [22] Fukutomi H, Iseki T, Endo T, Kamijo T. *Acta Metall Mater* 1991;39:1448.
- [23] Babcock SE, Balluffi RW. *Acta Metall* 1989;37:2367.
- [24] Winning M, Gottstein G, Shvindlerman LS. *Acta Mater* 2002;50:353–63.
- [25] Molodov D, Ivanov V, Gottstein G. *Acta Mater* 2007;55:1848.
- [26] Cahn J, Taylor J. *Acta Mater* 2004;52:4898.
- [27] Cahn J, Mishin Y, Suzuki A. *Philos Mag* 2006;86:3980.
- [28] Cahn J, Mishin Y, Suzuki A. *Acta Mater* 2006;54:4975.
- [29] Zhang K, Weertman J, Eastman J. *Appl Phys Lett* 2005;87.
- [30] Jin M, Minor A, Stach E, Morris J. *Acta Mater* 2004;52:5387.
- [31] Fan G, Fu L, Choo H, Liaw P, Browning N. *Acta Mater* 2006;54:4792.
- [32] Liao X, Kilmametov A, Valiev R, Gao H, Li X, Mukherjee A, et al. *Appl Phys Lett* 2006;88:021909.
- [33] Keller R, Geiss R, Barbosa N, Slifka A, Read D. *Metall Mater Trans A* 2007;38A:2272.
- [34] Kumar K, Van Swygenhoven H, Suresh S. *Acta Mater* 2003;51:5774.
- [35] Mughrabi H, Hoppel H, Kautz M, Valiev R. *Z Metall* 2003;94:1083.
- [36] Mughrabi H, Hoppel HW, Kautz M. *Scripta Mater* 2004;51:807–12.
- [37] Mullins WW. *Acta Metall* 1958;6:414.
- [38] Momprou F, Legros M, Caillard D. In: *MRS symp. proc.*, vol. 1086; 2008.
- [39] Humphreys F. *Scripta Metall Mater* 1992;27:1557–62.
- [40] Frost HJ, Thompson CV, Howe CL, Whang J. *Scripta Metall* 1988;22:65–70.
- [41] Zeng X, Li Y, Blum W. *Phys Status Solid A* 2004;201:R117.
- [42] Schiotz J. *Mater Sci Eng A* 2004;375–377:979.
- [43] Legros M, Gianola D, Hemker K. *Acta Mater* 2008;56:3393.